JOURNAL OF AIRCRAFT
Vol. 33, No. 5, September–October 1996

Divergent-Trailing-Edge Airfoil Flow

Brian E. Thompson* and Robert D. Lotz†
Rensselaer Polytechnic Institute, Troy, New York 12180-3590

The influence of recirculating flow on drag reduction associated with a divergent-trailing-edge (DTE) airfoil is provided by comparing the flow structure around a supercritical airfoil with a blunt trailing edge to that around the same airfoil after DTE modification. Flow characteristics are obtained by solution of compressible, Reynolds-averaged, Navier–Stokes equations with a linearized block implicit solution procedure and mixing-length turbulence model. Results show that DTE modification effects an increase in the streamwise length of the recirculation region downstream of a blunt trailing edge that acts like a chordwise extension to increase circulation. The divergent trailing edge gives the same lift at lower incidence and drag, so that lift-to-drag ratio is increased in transonic cruise. Drag creep is reduced by DTE modification because shock-induced drag is decreased as a result of a longer recirculation region in the wake and its associated relocation and weakening of the shock, which is greater than the increase in base drag.

Nomenclature

C_d = drag/$(\frac{1}{2}\rho U^2 c)$, sectional drag coefficient
C_l = lift/$(\frac{1}{2}\rho U^2 c)$, sectional lift coefficient
C_m = moment/$(\frac{1}{2}\rho U^2 c^2)$, sectional pitching moment coefficient
c = chord length
M = Mach number
q = dynamic pressure, $(\frac{1}{2}\rho U^2)$
Re = Reynolds number, Uc/ν
U, u = velocity
x, y, z = Cartesian coordinates
α = angle of attack
μ, ν = dynamic and kinematic viscosities

Introduction

THE current trend is towards commercial aircraft with higher cruising speeds in the transonic regime. Supercritical airfoils[1] are designed to have almost constant suction-side pressure, that is, a rooftop pressure distribution, and operate at higher subsonic cruise speeds because drag rise onset is at a higher Mach number than with conventional airfoils.[2] The rooftop design reduces camber upstream of the location of maximum thickness and increases camber near the trailing edge, which results in aft loading and larger negative (nose-down) pitching moments.[2,3]

Divergent-trailing-edge (DTE) modifications were designed to reduce drag on supercritical airfoils in transonic cruise.[4,5] Most subsonic airfoils have a sharp finite angle trailing edge to avoid drag. In practice, blunt trailing edges are used on the supercritical airfoils of many commercial aircraft, in part because these airfoils were designed to the aforementioned rooftop criterion, which results in suction- and pressure-side surfaces being almost parallel at the trailing edge. Use of a sharp trailing edge is structurally weak and the airfoil surfaces deflect under the high aft loading typical of supercritical airfoils, whereas blunt trailing edges offer improved strength, stiffness, manufacturing, and maintenance. At subsonic speeds, a blunt rather than sharp trailing edge results in minimal or negligible drag increase.[6]

Drag creep is the gradual increase in drag at speeds above 0.3 Mach caused by combined compressible and viscous effects. The cruise speed for a commercial aircraft is often chosen at the Mach number where $\partial(C_d)/\partial(M)$ is 0.1. Figure 1 shows that, first, drag creep on blunt supercritical airfoils is significant at the cruise speed and, second, a DTE modification[4] reduces drag creep and does not affect drag rise Mach number.

DTE airfoils are designed by modifying the upper and lower surfaces of a supercritical airfoil with blunt trailing edge to give both a divergent trailing-edge angle and an increasing curvature change towards the trailing edge, especially on the pressure side. Figure 2 shows the DLBA 243 airfoil produced by DTE modification of a DLBA 186 supercritical airfoil.[5] Wind-tunnel measurements[4] obtained for both airfoils are plotted on Fig. 1 and show significant reductions in drag creep at

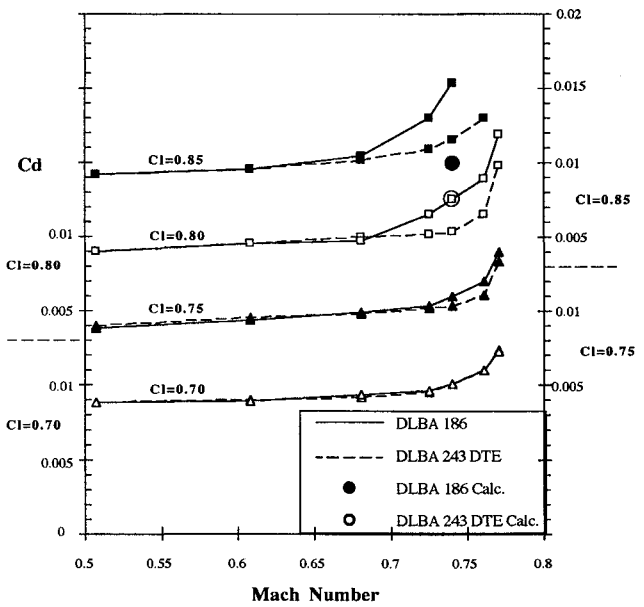

Fig. 1 Measured and calculated drag characteristics for DLBA 243 and DLBA 186 airfoils. (Measurement from Henne and Gregg.[4,5])

Received Nov. 28, 1994; revision received May 30, 1996; accepted for publication May 30, 1996.

*Associate Professor, Department of Mechanical Engineering, Aeronautical Engineering, and Mechanics. Member AIAA.

†Graduate Student, Department of Mechanical Engineering, Aeronautical Engineering, and Mechanics.

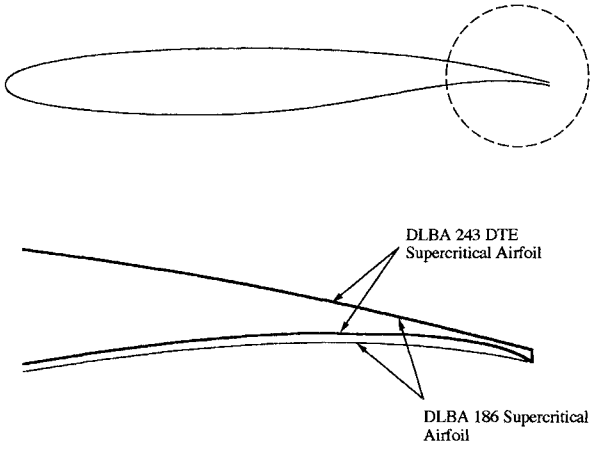

Fig. 2 Supercritical seed (DLBA 186) and DTE (DLBA 243) airfoils.

lift coefficients above 0.7 for the DTE airfoil. Comparison of measured pressure distributions[5] suggests DTE modification moves the suction-side shock aft, which further increases aft loading and nose-down pitching moment. However, the effects of DTE modification on the flow structure, especially the recirculating wake, are not well understood and are the subject of this research.

Previous experiments and calculations[4,5] with DTE airfoils have not focused on the nature of the recirculating flow in the wake and its importance to the design of DTE geometries. Measurements have not been reported in the small recirculation region downstream of the blunt, divergent trailing edge. Such measurements are difficult and expensive to obtain since, for example, if conventional instrumentation were used, a large transonic tunnel would be necessary to resolve distributions in a recirculation bubble with cross-stream dimensions of about 0.5% chord. Henne and Gregg[4,5] reported calculations of flow around DTE airfoils that were obtained by solving transonic and integral boundary-layer equations with the viscous–inviscid interaction procedure of Bauer et al.[7] In the trailing-edge region, the recirculation region was estimated with an approximate bubble-closure streamline, although viscous effects in this region are crucial to the determination of circulation and drag levels.[8,9]

The objective of this contribution is to provide insight into the relationship between the structure of the recirculating flow in the vicinity of the blunt trailing edge and the drag reduction measured for DTE airfoils. Because of the very small recirculation region at the airfoil trailing edge, the expense and difficulties in experiments mentioned previously, and previous successes discussed later that calculate flow structures similar to those around DTE airfoils, a computational approach was adopted here to further our understanding. The following section describes the present Navier–Stokes calculation procedure including solution algorithm, grid generation, boundary conditions, and turbulence model. Numerical uncertainty and grid dependence are also discussed. The following section presents comparisons with well-established experiments that benchmark transonic airfoil flow. The results section shows calculations of flow around baseline (DLBA 186) and DTE (DLBA 243) airfoils, and this article ends with summary remarks on the flow structure around DTE airfoils and its implications for design.

Computational Fluid Dynamics Procedure

Navier–Stokes methods have been used to calculate subsonic and transonic flow around airfoils. Subsonic flows over airfoils with trailing-edge separation have been calculated and compare well with experiments.[8,10–12] Boundary-layer flow that approaches separation can be represented with conventional boundary-layer approximations,[13] but downstream of separation Reynolds-averaged Navier–Stokes equations are required.[8] For calculations of flow in the trailing-edge region, viscous effects must be included, especially at higher angles of attack where the boundary layer remains attached[8]; effects of the wake and normal pressure gradients are significant, even at small incidence for attached flow[8]; simple turbulence models can be used for engineering design and to describe flow structures[8]; and, for conventional airfoils, the influence of trailing-edge thickness is confined to a small region at low angles of attack.[8] Viscous–inviscid interactive methods[14,15] solve integral or differential forms of boundary-layer equations coupled to potential-flow or Euler equations and, although these can been useful in commercial-airfoil design, the strong interaction between shock and boundary layer in the present flow makes solution of boundary-layer equations inappropriate.[3,9,16] For transonic airfoil flows with shock/boundary-layer[14–18] or vortex[19] interactions, solution of Reynolds-averaged Navier–Stokes equations are often preferred, because turbulence-model approximations replace profile and streamline-closure assumptions; the effects of the wake and normal pressure gradient, which are needed in the vicinity of recirculation,[8] are calculated; and the matching of solutions from different equations at internal boundaries is eliminated. This implies that calculations of airfoils with transonic and recirculation regions require solution of Navier–Stokes transport equations. Both of these features occur around blunt and DTE airfoils, and so the following Reynolds-averaged Navier–Stokes calculation procedure[20] was chosen for the present contribution.

Solution Algorithm

The two-dimensional, Reynolds-averaged, Navier–Stokes equations were solved here as described in Thompson and Lotz[21] using the linearized block implicit numerical procedure of Briley and McDonald,[20,22] which employs centered spatial differences with adjustable numerical dissipation.[19,20]

Turbulence Model Approximation

It was not the objective here to compare turbulence models, but rather to use a turbulence approximation that allows insight into the behavior of the mean flow around blunt and DTE airfoils, albeit with uncertainties in the turbulence structure. It is difficult to discriminate between the effects of turbulence-model, boundary-layer, and numerical approximations in calculations, and previous recommendations[14,16,18] have not provided an obvious choice for the complex flow around the blunt, transonic airfoils under consideration here. Calculations around blunt trailing-edge airfoils[23–25] show that a reasonable mean-flow structure can be obtained, although details of the effects of the turbulence model cannot be distinguished from those of numerical uncertainties. Mixing-length[11,26,27] and two-equation[8,10,26,28,29] turbulence models have been used successfully to calculate airfoil flows with small recirculation regions and, provided numerical accuracy is adequate, comparisons with experiment have been favorable.[8,29,30] However, the successes of Spalart[24] and Spalart and Allmaras[25] suggest that one equation models are appropriate airfoils flying at cruise conditions and, accordingly, was chosen here for the following reasons.

1) It is simple so that transport equations can be solved with minimal numerical uncertainty as discussed by Lotz and Thompson.[21]

2) Previous calculations with this turbulence model, the present numerical procedure, and adequate grid refinement have compared favorably with mean-flow velocities, and agreed well with the measured structure of the mean flow around airfoils, cascades, and turbine blades.[11,14,17,31]

3) The present airfoils are at incidence angles less than 2 deg with blunt trailing edges of about 0.0057 chord, which causes a recirculation region with cross-stream and streamwise dimensions of about 0.007 and 0.020 chord, respectively, in the downstream wake. The effects of turbulence in this tiny region are small compared to the influence of the boundary-

layer and compressible flow. Boundary-layer development and shock formation are not influenced by this tiny wake feature, except through the Kutta condition, which was well represented in previous calculations of transonic flow[17] and in steady and unsteady airfoil flows with separation.[11]

4) Previous comparisons between experiments and calculations with mixing-length and two-equation turbulence models in airfoil flows[11,17] and small, unconfined recirculating[8,12,28] flows provide no definitive preference, provided that numerical uncertainty is satisfactorily small. Lastly, the present calculation procedure is validated herein using both established transonic–airfoil experiments and results with supercritical and DTE airfoils: agreement is within 2% for lift and drag, and is discussed further. The present mixing-length model was calibrated for airfoils and provides Reynolds stresses in the boundary layer and wake as described by Lotz and Thompson.[21] The present model does not calculate transition, but rather fixes transition either at the location of boundary trips in wind-tunnel experiments or at the suction peak where laminar separation turbulent reattachment would be expected.[29] Upstream of this location, laminar viscosity was calculated with the Sutherland viscosity law.[20]

Boundary Conditions

At the inflow surface, the total pressure is associated with the streamwise momentum equation, the crossflow velocity components are set to zero, the second derivative of pressure is set equal to zero, and the stagnation enthalpy equals the reference total enthalpy. For the exit boundary and the upper and lower boundaries, the second derivative of the velocity components are set to zero, the pressure is specified, and the second derivative of the reference total enthalpy is set to zero. At the airfoil surface, no-slip conditions require each velocity component to be set equal to zero and the continuity equation to be solved. The wall is adiabatic with the change in enthalpy set equal to zero.[19]

Computational Mesh

Figure 3 shows a structured H-grid with nonuniform spacing, which is typical of that used here, and was created using EAGLE[32] grid generation software. Computational boundaries were expanded until their effect on the solution was negligible and they were located by trial and error at 100 chord lengths from the airfoil to the upper, lower, and exit boundaries, and 60 chord lengths upstream from the leading edge to the inflow boundary.

The calculation domain had 185 and 125 grid nodes in streamwise and cross-stream directions, respectively. In the streamwise direction, there are 35 points upstream of the leading edge, 90 points along the airfoil upper and lower surfaces from 0.06% of chord to the trailing edge, and 60 points downstream of the trailing edge to the exit boundary. Concentrations of 25 and 31 nodes were placed in the shock capture zone and in the blunt trailing-edge wake, respectively. In the cross-streamwise direction, 47 nodes were placed above and below the airfoil, and 29 nodes covered the thickness from 0.06% of chord on the suction to pressure side at the leading edge and across the blunt trailing edge. The shock capture zone was located by trial and error by centering it over the expected shock region and then refining and adjusting it until the shock remained within 0.2% of chord, despite shifts in the zone location of about 1% of chord.

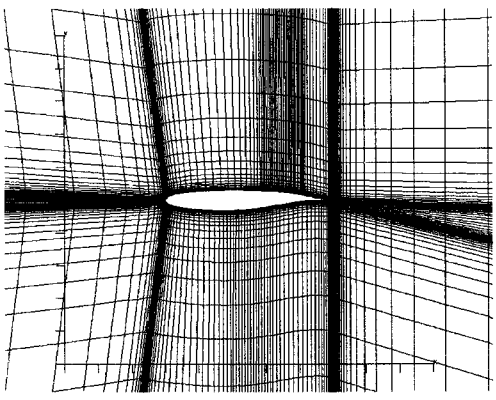

Fig. 3 Supercritical airfoil grid.

Grid spacing normal to the airfoil surface was 0.003% of chord at the wall and expanded according to a hyperbolic function towards the boundaries. This provided about 50 points to resolve the wake at the trailing edge. Calculations were obtained with wall spacings of 0.01 and 0.001% of chord at the wall, and all of the calculated distributions of boundary-layer velocity agreed within 1% for the RAE 2822 and DLBA airfoils presented next.

Numerical Uncertainty

Approximate quantification of numerical uncertainty was obtained with the method of Roache[34] described by Lotz and Thompson,[21] which indicates calculated values within 0.3 and 6% of lift and drag, respectively. These estimates[33] are obtained with the assumption that the solution for finer grids asymptotically approaches the correct solution, which is achieved in the limit of the spacing approaching zero.[33] Grid convergence index (GCI) based on Richardson number interpolation was calculated for uniform grid refinement, and gives a conservative error estimate for a second-order numerical method,[33] such as that used here. Results[21] show asymptotic convergence in aerodynamic coefficients and, for the 185 by 125 grid, the calculated value of GCI for the lift coefficient was 0.03%, which implies the 185 by 125 node grid is adequate and was used for the results presented next.

Validation Calculations for Blunt Supercritical Airfoils

Transonic flow around an RAE 2822 airfoil exhibits boundary-layer and shock characteristics similar to those on DTE airfoils. The benchmark RAE 2822 experiment[14,34] is used here to validate the aforementioned CFD procedure. Figure 3 shows an H-grid that is similar to the 185 × 125 grid used here for the RAE 2822 airfoil. The distribution and spacing of nodes, the outer computational boundaries, and the boundary conditions were implemented as described earlier. The upper and lower surfaces of the RAE 2822 were terminated at 99% of the chord to give a blunt trailing-edge thickness of 0.0017 chord. Table 1 presents calculated and measured results for the RAE 2822 airfoil at the experimental test conditions of 3.22-deg incidence, 0.728 Mach number, and $Re = 6.5 \times 10^6$, and with transition fixed at 3% of chord to match the location of trip sandpaper in the experiment. The best match of the experimental pressure distribution was obtained at 2.95-deg incidence, 0.728 Mach number, and $Re = 6.5 \times 10^6$, which are within the reasonable bounds of the reported experimental uncertainty. Calculated lift and drag were about 1.7 and 2.1% higher than measured values, whereas calculated lift-to-drag ratio was fortuitously within 1% of measured values. Figure 4 compares measured and calculated values of pressure coefficient, which were within 0.04 except in the immediate vicinity of the shock.

Results

Calculations are presented here for the DLBA 186 (seed) and DLBA 243 (DTE) supercritical airfoils with trailing-edge thicknesses of 0.57% of chord shown in Fig. 2. Table 1 quantifies calculated and measured lift and drag coefficients, lift-to-drag ratio, and shock location for a chosen set of angles of attack and Mach numbers for both DTE and seed airfoils. Calculated distributions of velocity and pressure are presented

Table 1 Calculated and measured aerodynamic coefficients

Airfoil	Angle of attack	Mach number	Reynolds number	Lift coefficient	Drag coefficient	L/D ratio	Shock location, % of chord
			Measurements by Kline et al.[34]				
RAE 2822	3.22	0.728	6.50E+06	0.802	0.0175	45.8	50
			Calculation				
RAE 2822	2.95	0.728	6.50E+06	0.817	0.0179	45.6	50
			Measurement by Henne and Gregg[4,5]				
DLBA 186	1.809	0.74	1.45E+07	0.813	0.0122	66.6	50
DLBA 243	0.904	0.74	1.45E+07	0.805	0.0101	79.7	50
			Calculation				
DLBA 186	1.429	0.726	1.45E+07	0.803	0.0129	62.2	50
DLBA 243	1.429	0.726	1.45E+07	0.982	0.0182	54	62
DLBA 243	0.6	0.726	1.45E+07	0.801	0.0125	64.1	58

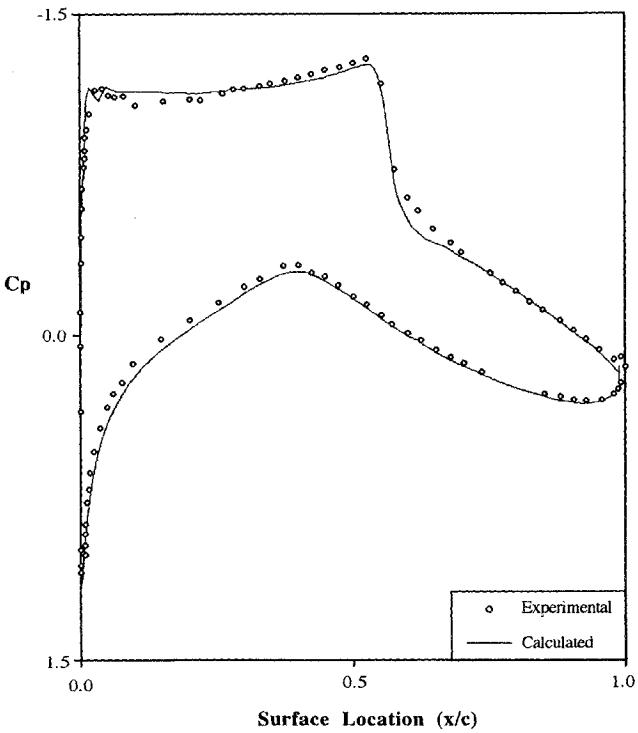

Fig. 4 Calculated and measured distributions of surface pressure on an RAE 2822 airfoil at C_l = 0.80 (measurements from Kline et al.[34]).

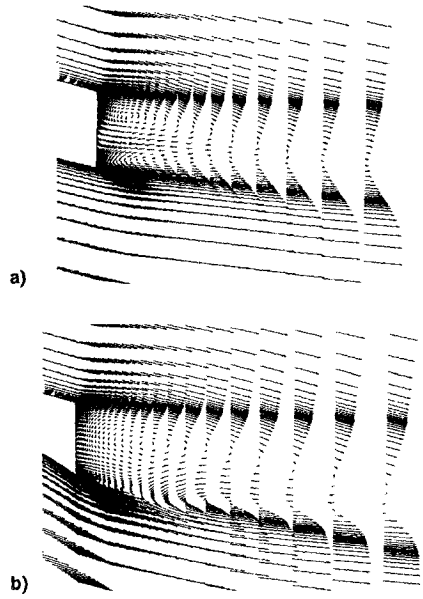

Fig. 5 Calculated distributions of velocity in the trailing edge region of DLBA 186 and 243 airfoils at M = 0.726, Re = 14.5 × 10^6, and C_l = 0.80: a) seed DLBA 186 airfoil, C_d = 0.0129 and b) DTE DLBA 243 airfoil, C_d = 0.0125.

next to explain these choices and to provide insight into the flow structures that result in reduction of drag creep with DTE airfoils.

Seed (DLBA 186) Airfoil Calculations and Comparison with Experiment

Flow around the DLBA 186 airfoil was calculated for the experimental conditions reported by Henne and Gregg,[4,5] which were incidence of 1.809 deg, transition fixed at 5% of chord where the boundary-layer trip wire was located in the experiment, Mach number of 0.740, and Re = 14.5 × 10^6.

Maximum uncertainties in the measured values of incidence and Mach number were reported by Henne and Gregg[4] to be about 0.4 and 0.02 deg, respectively, and this is consistent with our experience with the two-dimensional section and associated instrumentation of the NAE 5 × 5 ft transonic wind tunnel in which these DLBA airfoil measurements were made. The previous calculations were repeated with incidence adjusted until the calculated lift matched the measured lift coefficient of 0.8 at the reported Mach and Reynolds numbers. The best overall agreement in the pressure distribution and lift coefficient was obtained at 1.429-deg incidence and 0.726 Mach number. Drag coefficients agreed within 5% and shock locations matched within 0.3% of chord. The pressure-side distribution of surface pressure is in excellent agreement. Figure 5 shows the calculated velocity vectors in the wake that depict a recirculation region with a well-defined clockwise vortex situated above a counterclockwise vortex that extends approximately 2% of chord downstream into the wake.

Comparison with DTE (DLBA 243) Airfoil Calculations

The grid used for this airfoil is almost identical to the DLBA 186 grid: the exception is the concentration of nodes in the shock capture zone that is located appropriately around the shock and further aft on the upper surface. Figure 6 compares distributions of surface pressure on the DLBA 186 and 243 airfoils both at 1.429-deg incidence and a lift coefficient of 0.80, and calculated at Mach and Reynolds numbers of 0.726 and 14.5 × 10^6, respectively. At the same angle of incidence, the shock on the DLBA 243 is stronger and farther downstream. The pressure difference between suction and pressure side across the aft end of the DTE airfoil is approximately

constant from the shock to the trailing edge. Surface pressures on both suction and pressure sides of the DTE airfoil envelop those of the seed airfoil, which indicates greater circulation and, consequently, the lift coefficient is about 20% greater. Drag is about 50% greater because of the increased shock strength. Figure 5 compares velocity vectors in the near-wake region, which shows the recirculation regions extend about 2 and 4% of chord into the wake of DLBA 186 and 243 airfoils, respectively. The DLBA 243 flow has a larger clockwise vortex situated on the suction side of the recirculation bubble and a more elongated counterclockwise vortex compared to that on the DLBA 186.

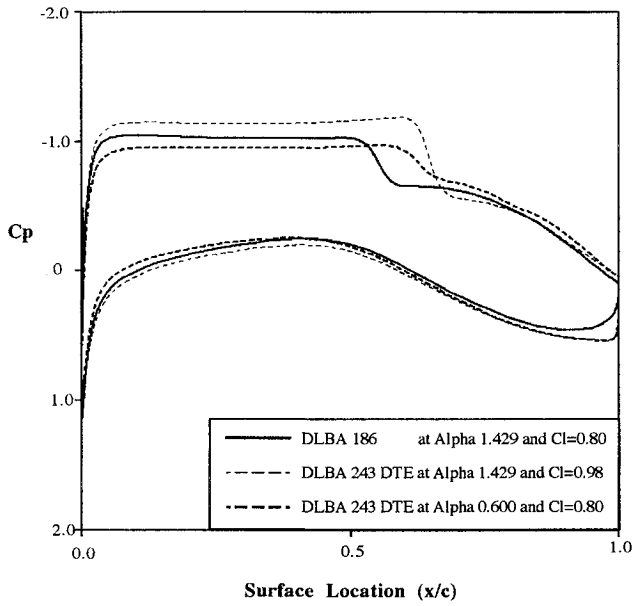

Fig. 6 Calculated distribution of surface pressure on DLBA 186 and 243 airfoils at $M = 0.726$ and $Re = 14.5 \times 10^6$.

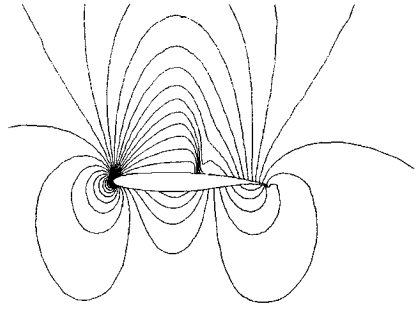

Fig. 7 Calculated distribution of pressure around the DLBA 186 airfoil at $M = 0.726$, $Re = 14.5 \times 10^6$, and $C_l = 0.80$ ($\Delta cp = 0.02$ between contours).

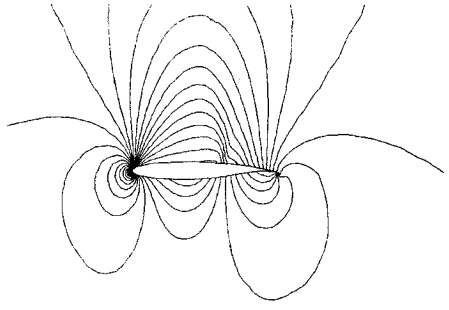

Fig. 8 Calculated distribution of pressure around the DLBA 243 airfoil at $M = 0.726$, $Re = 14.5 \times 10^6$, and $C_l = 0.80$ ($\Delta cp = 0.02$ between contours).

The benefit of a DTE modification[5] is to increase lift-to-drag ratio, that is, to decrease drag at the cruise lift coefficient. This suggests the fair comparison between DTE and seed airfoil is at different angles of attack that produce the same lift coefficient. The cruise lift coefficient for the DLBA airfoils is 0.8 and, for the DLBA 186 airfoil, was calculated at 1.429-deg incidence and 0.726 Mach. Henne and Gregg[4,5] measured a lift coefficient of 0.8 at 0.904 deg incidence of the DLBA 243 airfoil, but Table 1 shows this incidence did not produce this lift in calculations: this is attributable to incidence and Mach number uncertainties mentioned previously with the DLBA 186 airfoil. Tunnel operating conditions were maintained at 0.726 Mach and $Re = 14.5 \times 10^6$, and calculations were repeated with the DLBA 243 airfoil at 0.600-deg incidence for a calculated lift coefficient of 0.8. This is a difference in incidence of about 0.3 deg and again within the previous experimental uncertainty limits reported by Henne and Gregg.[4]

Figure 6 also compares the calculated values of surface pressure at a lift coefficient of 0.80 with the DLBA 186 and 243 airfoils at 1.429- and 0.600-deg incidence, respectively. The DTE airfoil has a weaker and delayed shock when compared to the seed airfoil. The supercritical region of the DTE airfoil is not as intense and is diffused in the streamwise direction compared to that of the DLBA 186 airfoil. The difference in pressure from suction- to pressure-side of the DLBA 243 is again approximately constant from the shock to the trailing edge. Table 1 shows that, at the same lift coefficient, the lift-to-drag ratio for the DLBA 243 is about 3% higher than for the DLBA 186 airfoil. Figure 7 shows velocity vectors in the trailing-edge region and the DTE recirculation region again extends about 4% of the chord downstream with similar vortex structure as calculated earlier at the higher angles of attack.

Figures 7 and 8 compare distributions of calculated pressures around the DLBA 186 and 243 airfoils at the design lift coefficient of 0.8. The shock starts in the boundary layer and extends normal to the surface about 0.5 chord into the freestream. Calculated pressure recovers slightly behind the shock on the DLBA 186 suction-side, although this recovery does not reach the surface of the airfoil and therefore does not appear in the distribution of surface pressure coefficient shown in Fig. 10. Measured surface pressures[5] show a slight recovery just behind the shock, and it is believed that the wall-boundary conditions damped this effect in the calculations. The recovery to subsonic flow is more gradual over the DTE airfoil than over the seed DLBA 186 airfoil.

Conclusions

The calculated results presented here are subject to uncertainties that result from numerical, boundary-condition, and turbulence-model assumptions that are difficult to isolate. Uncertainties associated with boundary conditions and mesh densities are estimated previously to contribute less than 0.3% to lift and 6% to drag based on the grid studies reported earlier. Measured and calculated flow structures, sensibly describe the shock, boundary layer, and the recirculating flow, and, in combination with the cited experiments, provide insights that lead to the following statements.

Comparison of calculations of DTE (DLBA 243) and seed (DLBA 186) airfoils at the same Reynolds and Mach number, shows the following:

1) At the same angle of attack, DTE airfoils can have lift and drag increases of 20 and 50%, respectively.

2) At the same lift coefficient, drag creep can be reduced at transonic cruise speeds on supercritical airfoils by DTE modification. There is an improvement in lift-to-drag ratio that is calculated here to be about 3%.

3) Pressure difference between the pressure- and suction-side of DTE airfoils is constant from the suction-side shock aft to the trailing edge.

4) DTE modification reduced the size of the region affected by compressibility and weakened the suction-side shock compared to those around the seed supercritical airfoil.

5) For the present airfoils with blunt trailing edges of thickness 0.0057 chord, DTE modification increased the streamwise length of the recirculation region downstream of the blunt trailing edge to about 4% of chord from about 2% for the seed supercritical airfoil.

The benefit of DTE modification is an increase in lift-to-drag ratio for a given lift coefficient at transonic cruise speeds. The increased circulation associated with the DTE modification results in flight at lower angles of attack to obtain the same lift as the seed supercritical airfoil. DTE modification causes an increase in base drag, which is associated with the larger trailing-edge recirculation region, but this increase is less than the drag decrease resulting from the weakened shock. When designing DTE airfoils, the trailing-edge recirculation should be lengthened in the downstream wake to act like a chord extension that increases circulation, and then the designer should optimize the tradeoff between shock-induced and base drag.

References

[1]Whitcomb, R. T., "Review of NASA Supercritical Airfoils," *Proceedings of the 9th International Congress of the International Council of the Aeronautical Sciences (ICAS)*, Hampton, VA, 1974 (Paper 11.1).

[2]Ayers, T. G., "Supercritical Aerodynamics-Worthwhile over a Range of Speeds," *Astronautics & Aeronautics*, Vol. 41, Aug. 1972, pp. 32–36.

[3]Hurley, F. X., Spaid, F. W., Roos, F. W., Stivers, L. S., Jr., and Bandettini, A., "Supercritical Airfoil Flowfield Measurements," *Journal of Aircraft*, Vol. 12, No. 9, 1975, pp. 737–744.

[4]Henne, P. A., and Gregg, R. D., "New Airfoil Design Concept," *Journal of Aircraft*, Vol. 28, No. 5, 1991, pp. 300–311.

[5]Henne, P. A., "Innovation with Computational Aerodynamics: The Divergent Trailing-Edge Airfoil," *Applied Computational Aerodynamics*, edited by P. A. Henne, AIAA Education Series, AIAA, Washington, DC, 1990, pp. 221–262.

[6]Harris, C. D., "Wind Tunnel Investigation of Effects of Trailing Edge Geometry on a NASA Supercritical Airfoil Section," NASA TM-X-2336, Jan. 1971.

[7]Bauer, F., Garabedian, P., Korn, D., and Jameson, A., *Supercritical Wing Sections II, Lecture Notes in Economics and Mathematical Systems*, Vol. 108, Springer–Verlag, New York, 1975.

[8]Thompson, B. E., and Whitelaw, J. H., "Trailing-Edge Region of Airfoils," *Journal of Aircraft*, Vol. 26, No. 3, 1989, pp. 225–234.

[9]Melnik, R. E., Chow, R., and Mead, H. R., "Theory of Viscous Transonic Flow over Airfoils at High Reynolds Number," AIAA Paper 77-680, June 1977.

[10]Thompson, B. E., and Reis, L., *Comparison of Finite Difference Calculations of a Large Region of Recirculating Flow near the Trailing Edge of an Airfoil*, edited by L. Ohman, CP 412, AGARD, 1986.

[11]Shamroth, S. J., and Gibeling, H. J., "Navier-Stokes Solution of the Turbulent Flow Field About an Isolated Airfoil," *AIAA Journal*, Vol. 18, No. 3, 1980, pp. 1409–1413.

[12]Adair, D., Thompson, B. E., Whitelaw, J. H., and Williams, B. R., "Comparison of Interactive and Navier-Stokes Calculations for Separated Flows," *Numerical and Physical Aspects of Aerodynamic Flows III*, edited by T. Cebeci, Springer–Verlag, New York, 1986.

[13]Thompson, B. E., and Whitelaw, J. H., "A Turbulent Boundary Layer Approaching Separation," *Walz-Festschrift Volume*, Springer–Verlag, New York, 1983, pp. 253–262.

[14]Locke, R. C., and Williams, B. R., "Viscous-Inviscid Interactions in External Aerodynamics," *Progress of Aerospace Science*, Vol. 24, No. 1, 1987, pp. 51–76.

[15]Spreiter, J. R., "Transonic Aerodynamics—History and Statement of the Problem," *Transonic Aerodynamics*, edited by D. Nixon, AIAA Education Series, New York, 1981, pp. 3–80.

[16]Johnson, D. A., and Spaid, F. W., "Supercritical Airfoil Boundary-Layer and Near-Wake Measurements," *Journal of Aircraft*, Vol. 20, No. 4, 1983, pp. 298–305.

[17]Roscoe, D. V., Gibeling, H. J., McDonald, H., and Shamroth, S. J., "Development of a Navier-Stokes Analysis to Investigate the Mechanism of Shock-Wave-Boundary-Layer Interactions," *Numerical and Physical Aspects of Aerodynamic Flows III*, edited by T. Cebeci, Springer–Verlag, New York, 1985.

[18]Khan, M. M. S., Inger, G. R., and Lekoudis, S. G., "Computation of Transonic Flow Around Airfoils with Trailing Edge and Shock/Boundary Layer Interactions," *Journal of Aircraft*, Vol. 21, No. 6, 1984, pp. 380–388.

[19]Liu, N.-S., Davoudzadeh, F., Briley, W. R., and Shamroth, S. J., "Navier-Stokes Simulation of Transonic Blade-Vortex Interactions," *Journal of Fluids Engineering*, Vol. 112, Dec. 1990, pp. 501–509.

[20]Briley, W. R., and McDonald, H., "Solution of the Multi-Dimensional Compressible Navier-Stokes Equations by a Generalized Implicit Method," *Journal of Computational Physics*, Vol. 24, No. 1, 1977, pp. 372–397.

[21]Lotz, R. D., Thompson, B. E., Davoudzadeh, F., and Konings, C., "Grid Independence and Numerical Uncertainty Analysis of a Transonic Supercritical Airfoil Calculation," RWJ-10-94, Joint JSME/ASME Fluids Engineering Conf., Aug. 1995.

[22]Briley, W. R., and McDonald, H., "On the Structure and Use of Linearized Block Implicit Schemes," *Journal of Computational Physics*, Vol. 34, No. 1, 1980, pp. 54–73.

[23]Stanaway, S. K., McCroskey, W. J., and Kroo, I. M., "Navier-Stokes Analysis of Blunt Trailing Edge Airfoils," AIAA Paper 92-0024, Jan. 1992.

[24]Spalart, P. R., "Topics in Industrial Viscous Flow Calculations," Colloquium: Transitional Boundary Layers in Aeronautics, Royal Netherlands Academy of Arts and Sciences, Dec. 1995.

[25]Spalart, P. R., and Allmaras, S. R., "A One-Equation Turbulence Model for Aerodynamic Flows," *La Recherche Aerospaciale*, No. 1, 1994, pp. 5–21.

[26]Holst, T. L., "Viscous Transonic Airfoil Workshop Compendium of Results," *Journal Aircraft*, Vol. 25, No. 12, 1988, pp. 1108–1114.

[27]Micheltree, R. E., Salas, M. D., and Hassan, H. A., "One-Equation Turbulence Model for Transonic Airfoil Flows," *AIAA Journal*, Vol. 28, No. 9, 1990, pp. 321–325.

[28]Adair, D., Thompson, B. E., and Whitelaw, J. H., "Measurements and Calculations of a Separating Boundary-Layer and the Downstream Wake," *Numerical and Physical Aspects of Aerodynamic Flows II*, edited by T. Cebeci, Springer–Verlag, New York, 1984, pp. 92–111.

[29]Thompson, B. E., and Whitelaw, J. H., "Characteristics of a Trailing-Edge Flow with Turbulent Boundary-Layer Separation," *Journal of Fluid Mechanics*, Vol. 157, No. 1, 1985, pp. 305–326.

[30]Simpson, R. L., Chew, Y.-T., and Shivaprasad, B. G., "The Structure of a Turbulent Separating Boundary Layer," *Journal of Fluid Mechanics*, Vol. 113, No. 1, 1981, pp. 23–26.

[31]Mehta, U., and Lomax, H., "Reynolds Averaged Navier-Stokes Computations of Transonic Flows—the State-of-the-Art," *Transonic Aerodynamics*, edited by D. Nixon, AIAA Education Series, AIAA, New York, 1981, pp. 297–375.

[32]Thompson, J. F., *EAGLE User Manual 1988*, Mississippi State Univ., Mississippi State, MS, 1988.

[33]Roache, P. J., "A Method for Uniform Reporting of Grid Refinement Studies," *Quantification of Uncertainty in Computational Fluid Dynamics*, FED-Vol. 158, American Society of Mechanical Engineers, New York, 1993, pp. 109–120.

[34]Kline, S. J., Cantwell, B. J., and Lilley, G. M. (eds.), "1980–81 AFOSR-HTTM-Stanford Conference on Complex Turbulent Flows: Comparison of Computation and Experiments," Stanford Univ., Thermosciences Div., Mechanical Engineering Dept., Stanford, CA, Sept. 1980.